ARTICLES

Solvent Mediated Intramolecular Photoinduced Electron Transfer in a Fluorene-Perylene Bisimide Derivative

Edda E. Neuteboom, Stefan C. J. Meskers, Edwin H. A. Beckers, Stéphanie Chopin, and René A. J. Janssen*

Molecular Materials and Nanosystems, Eindhoven University of Technology, P.O. Box 513, 5600 MB Eindhoven, The Netherlands

Received: March 28, 2006; In Final Form: September 17, 2006

Photoinduced electron transfer from fluorene to perylene bisimide has been studied for 2,7-bis(*N*-(1-hexylheptyl)-3,4:9,10-perylene-bisimide-*N*'-yl))-9,9-didodecylfluorene (PFP) in 11 different organic solvents. The intramolecular charge-separated state in PFP is almost isoenergetic with the locally excited state of the perylene bisimide. As a consequence of the small change in free energy for charge separation, the electron transfer rate strongly depends on subtle changes in the medium. The rate constant k_{CS} for the electron transfer from fluorene to perylene bisimide moiety in the excited state varies over more than 2 orders of magnitude ($\sim 10^8-10^{10}$ s^{-1}) with the solvent but does not show the familiar increase with polarity. The widely differing rate constants can be successfully explained by considering (1) the contribution of the polarization energy of the dipole moment in the transition state and by (2) the classical Marcus-Jortner model and assuming a spherical cavity for the charge-separated state. Using the first model, we show that lnk_{CS} should vary linearly with Δf [$\Delta f = (\epsilon_r - 1)/(2\epsilon_r + 1) - (n^2 - 1)/(2n^2 + 1)$, where ϵ_r and n represent the static dielectric constant and the refractive index of the solvent, respectively], in accordance with experimental results. The second model, where the reorganization energy scales linearly with Δf, provides quantitative agreement with experimental rate constants within a factor of 2.

1. Introduction

Donor−acceptor compounds are actively considered as models for molecular solar energy conversion and artificial photosynthesis. In many investigations, creation of (supra)molecular architectures providing a long-living charge-separated state after absorption of light has been an important objective because these may allow charges to be collected in an external circuit or used in chemical reactions.[1] One of the successful strategies in this respect are arrays with multiple carefully positioned photoactive and electroactive groups in which photogenerated charges are spatially separated via a cascade of electron-transfer reactions after absorption of light.[2] The recombination of the electron and hole to the ground state is then inhibited by an extremely low electronic coupling of the distant wave functions of the electrons and holes. While the quantum efficiency of such a cascaded charge transfer process can be very high (95% in the photosynthetic reaction center), it usually involves significant but unfavorable energetic losses. In this respect, there is a direct relation between the free energy of the charge separated state and the maximum open-circuit voltage in an organic solar cell based on the same donor and acceptor chromophores. The open-circuit voltage is one of the crucial parameters that determine the energy conversion efficiency of these devices, and it is directly related to the energy of the charge-separated state between *p* and *n* type material.[3] To preserve the photon energy after charge separation, the energy of the charge-separated state should be as high as possible, and consequently the free energy liberated in the electron-transfer reaction should be small. Hence, for future organic solar cells and photosynthetic systems, it is of profound interest to establish conditions for photoinduced electron transfer in donor−acceptor systems with such a small driving force for charge transfer.

In this study we address photoinduced electron transfer in a donor−acceptor system where the difference between redox potentials of the two chromophores and the energy of the singlet excited state is small. The model system that we use (PFP, Figure 1) incorporates a fluorene donor and two perylene bisimide acceptors. Various perylene (bis)imide and (poly)fluorene conjugates have previously been reported in the literature. Some exhibit photoinduced electron transfer, while others show energy transfer followed by fluorescence of the perylene (bis)imide chromophore. The discrimination between electron and energy transfer in these systems depends on subtle differences in the distance between donor and acceptor, redox potentials, and the nature of the medium. Photoinduced energy transfer has been observed in systems where perylene monoimide serves as end capper of oligo- or polyfluorenes,[4] as pendant side chain,[4b,5] and for perylene bisimide incorporated in the main chain.[6] Also for oligofluorenes ($n = 1-3$) directly coupled to 1,7-bis(3,5-di-*tert*-butylphenoxy)perylene bisimides intramolecular photoinduced electron transfer is absent.[7] On the other

* To whom correspondence should be addressed. E-mail: r.a.j.janssen@tue.nl.

10.1021/jp061905n CCC: $33.50
Published on Web 10/25/2006

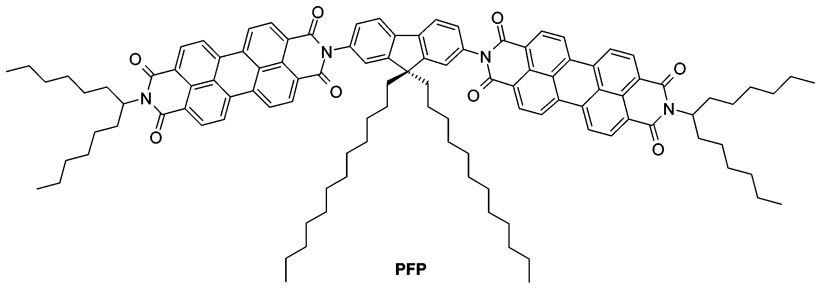

Figure 1. Structure of 2,7-bis(*N*-(1-hexylheptyl)-3,4:9,10-perylene-bisimide-*N*′-yl))-9,9-didodecylfluorene (PFP).

SCHEME 1: Synthesis of PFP and 5

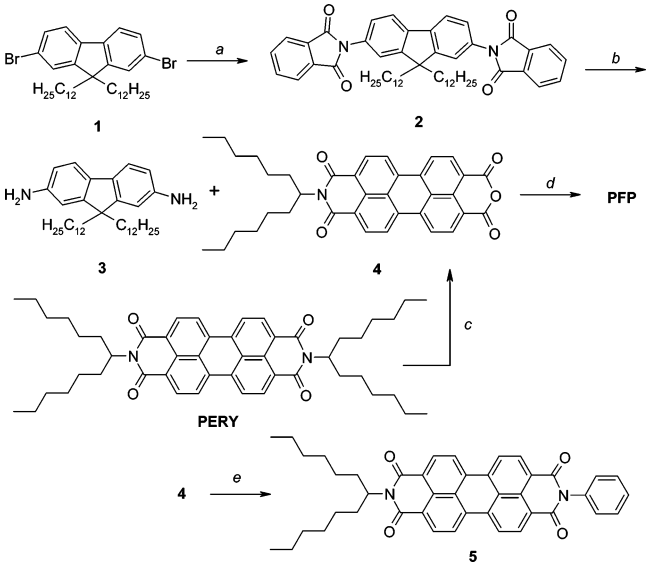

[a] Potassium phthalimide, CuI, DMA, 180 °C, 28%. [b] $N_2H_4 \cdot H_2O$, ethanol, reflux, 83%. [c] 1. KOH, *tert*-butyl alcohol, 2. HCl, 53%. [d] Imidazole, $Zn(OAc)_2$, 180 °C, 24%. [e] Aniline, imidazole, 140 °C, 74%.

hand, intramolecular photoinduced electron transfer has been observed for a perylene monoimide attached to a rigid substituted bisfluorene containing a *para*-coupled pentaphenyl moiety.[8] Likewise, charge transfer occurs in the excited state for a system similar to PFP where fluorene is coupled to an unsubstituted perylene bisimide.[9] The latter molecule is related to a series of perylene bisimide-oligophenylene-perylene bisimide triads that has been studied by Adams et al. for varying lengths of the oligophenylene bridge.[10] For these molecules, intramolecular photoinduced charge transfer was reported in which the electron is thought to be transferred from one perylene bisimide to the other over the bridge, while the alternative interpretation that the oligophenylenes act as electron donor was not considered explicitly.

Here we show that in PFP intramolecular photoinduced electron transfer from fluorene to the perylene bisimide is extremely sensitive to the environment. The effects of solvent and the dielectric properties on charge transfer reactions have been extensively described in the literature.[11] We rationalize the effects of the medium on the electron-transfer rate in terms of the polarization energy of the transition state using a dielectric continuum model with a spherical cavity.

2. Results

Synthesis. The synthesis of PFP is outlined in Scheme 1. First, 9,9-didodecyl-2,7-dibromofluorene **1** was reacted with potassium phthalimide in dimethylacetamide in the presence of copper(I) iodide to form bisphthalimide fluorene **2**.[12] Diaminofluorene **3** was synthesized by reaction of **2** with hydrazine monohydrate. 1-Hexylheptylamine, synthesized in a two-step procedure as reported by Semenov and Skorovarov,[13] was reacted with 3,4,9,10-perylenetetracarboxylic dianhydride in imidazole to *N*,*N*′-bis(1-hexylheptyl)-3,4:9,10-perylenedicarboximide (PERY) and then converted into **4** by reaction with KOH and subsequently HCl as described by Langhals et al.[14] PFP was obtained by reaction of monoanhydride **4** with the diaminofluorene **3** and was purified by column chromatography and preparative HPLC. Compound **5** was synthesized from **4** and aniline according to literature procedures.[15]

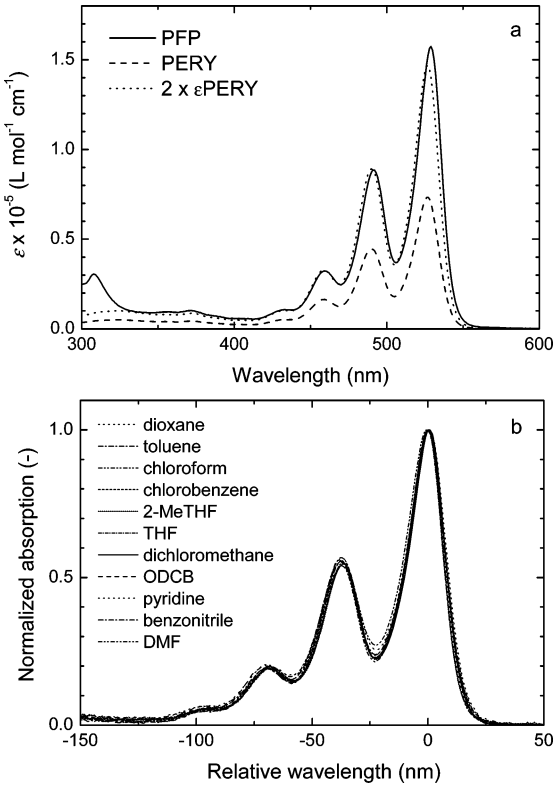

Figure 2. (a) UV/vis absorption spectra and molar absorption coefficients of PFP (solid line) and PERY (dashed line) in toluene solution. The dotted line pertains to the molar absorption coefficient of PERY, after multiplication by a factor 2. (b) UV/vis absorption spectra of PFP in 11 different solvents relative to the wavelength of maximum absorption λ_{max}.

UV/vis Absorption. In toluene solution the UV/vis absorption spectrum of PFP exhibits characteristic bands at 308, 459, 491, and 529 nm (Figure 2a). The band at 308 nm originates from the fluorene moiety, while the others are the vibronic bands of the perylene bisimide $S_1 \leftarrow S_0$ transition. In the long wavelength region, the absorption spectra of PFP and the PERY reference compound are almost identical, demonstrating that the three chromophores in PFP are electronically only weakly coupled as a consequence of the twisted conformation around the

TABLE 1: Absorption and Fluorescence Energies ν_{max} (eV) of PERY and PFP Together with the Relative Dielectric Constant ϵ_r, Refractive Index n, and Solvent Parameters, f, f', Δf, and λ_s (eV)

	PERY		PFP		solvent parameters					
solvent	abs ν_{max}	PL ν_{max}	Abs ν_{max}	PL ν_{max}	ϵ_r	n	f[a]	f'[b]	Δf[c]	λ_s[d]
dioxane	2.371	2.340	2.366	2.340	2.27	1.422	0.229	0.203	0.027	0.14
toluene	2.353	2.318	2.344	2.309	2.38	1.479	0.239	0.221	0.019	0.10
chloroform	2.353	2.324	2.344	2.318	4.81	1.446	0.359	0.211	0.148	0.77
chlorobenzene	2.344	2.309	2.335	2.305	5.69	1.525	0.379	0.235	0.144	0.75
2-MeTHF	2.380	2.348	2.371	2.344	6.97	1.408	0.400	0.198	0.202	1.05
THF	2.375	2.340	2.366	2.335	7.47	1.406	0.406	0.197	0.209	1.08
DCM	2.362	2.331	2.353	2.322	8.93	1.424	0.420	0.203	0.217	1.13
ODCB	2.335	2.301	2.326	2.292	9.93	1.551	0.428	0.242	0.186	0.97
pyridine	2.340	2.301	2.331	2.292	12.3	1.51	0.441	0.230	0.211	1.10
benzonitrile	2.340	2.305	2.331	2.296	25.2	1.529	0.471	0.236	0.235	1.22
DMF	2.357	2.313	2.348	2.309	37.1	1.43	0.480	0.205	0.275	1.43

[a] $f = (\epsilon_r - 1)/(2\epsilon_r + 1)$. [b] $f' = (n^2 - 1)/(2n^2 + 1)$. [c] $\Delta f = f - f'$. [d] λ_s from eq 12.

fluorene-perylene bisimide carbon−nitrogen bonds.[9] In accordance, the molar absorption coefficient of PFP (15.7×10^4 L mol^{-1} cm^{-1}) is approximately twice that of PERY (7.3×10^4 L mol^{-1} cm^{-1}).

UV/vis spectra of PFP and PERY were further recorded in 11 different organic solvents with varying dielectric constants (Figure 2b). The wavelength of maximum absorption (λ_{max}) of PFP varies with the solvent, ranging from 523 nm in 2-MeTHF to 533 nm in *o*-dichlorobenzene (ODCB). Table 1 lists the transition energies ($\nu_{max} = hc/\lambda_{max}$) for both PFP and PERY and reveals that the solvatochromic behavior of PFP is virtually identical to that of PERY. When corrected for the small differences in λ_{max}, the absorption spectra of PFP are almost identical in all 11 solvents (Figure 2b). No significant difference in relative height or width of the vibronic absorption bands exists. Since it is well established that the formation of aggregates of perylene bisimides results in significant changes in relative intensities of the bands,[16] we exclude the possibility that aggregation of PFP occurs or differs strongly among these solvents. Since the absorption spectra of PFP overlap very well with those of molecularly dissolved (i.e. not aggregated) PERY (Figure 2a), we conclude that aggregation of PFP does not take place at the concentrations used.

Electrochemistry. Cyclic voltammetry of PFP in dichloromethane (DCM) revealed two reversible reduction waves at $E_{red}(1) = -1.075$ V and $E_{red}(2) = -1.278$ V vs Fc/Fc$^+$ (Figure 3). PFP also shows two oxidation waves at $E_{ox}(1) = 1.247$ V and $E_{ox}(2) = 1.452$ V. The current associated with the last wave is approximately half of the current of the three other redox waves. Apart from this last wave, reference compound **5** exhibits almost identical redox potentials (Figure 3, $E_{red}(1) = -1.065$ V, $E_{red}(2) = -1.265$ V, and $E_{ox}(1) = 1.252$ V) as PFP which establishes that each of the corresponding redox processes in PFP are each two-electron reductions or oxidations, involving the two perylene bisimides. Consequently, the $E_{ox}(2)$ of 1.452 V for PFP is likely associated with a single-electron oxidation of the fluorene unit of PFP. Unsubsitituted fluorene itself, however, has a significantly lower oxidation potential and shows an irreversible wave with a peak potential at 1.300 V (Figure 3).[17] We stress that cyclic voltammetry overestimates the ionization potential of the fluorene unit in PFP because the redox wave at 1.452 V is associated with the $PFP^{2+} \rightarrow PFP^{3+}$ reaction, rather than with the oxidation of the fluorene moiety in a neutral PFP. Coulomb repulsion will place the $PFP^{2+} \rightarrow PFP^{3+}$ process at a higher potential. The potential increase due two charging can be calculated from $\Delta E = 2e/4\pi\epsilon_0\epsilon_r d$, where d is the distance between the positive charge located in the center of the fluorene and centers of positive charge density in the perylene bisimides. The factor of 2 accounts for the fact that a positive charge in each of the two perylene bisimides moieties contributes to the repulsion. The experimental potential increase of $\Delta E \approx 1.45 - 1.25 = 0.20$ V in DCM ($\epsilon_r = 8.93$) gives an estimate for d of 16 Å that corresponds to half the length PFP suggesting that the three positive charges tend to maximize their distance. To ensure that the imide moieties themselves are not responsible for the increased oxidation potential, we also checked the oxidation of **2**. The 2,7-substitution of the fluorene moiety in reference **2** resembles the one in PFP. Compound **2** already oxidizes at $E_{ox}(1) = 1.146$ V (Figure 3), which is at a lower potential than fluorene itself. In conclusion, there is some ambiguity on the precise oxidation potential of the fluorene unit in neutral PFP, but the above analysis shows that a value of +1.25 V vs Fc/Fc$^+$ is a realistic estimate.

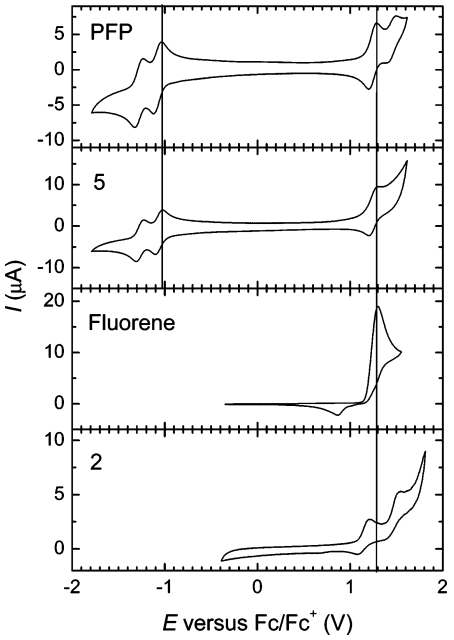

Figure 3. Cyclic voltammograms of PFP, **5**, fluorene, and **2** recorded in dichloromethane. Vertical lines allow comparison of first oxidation and reduction potentials.

Fluorescence. Fluorescence spectra of PFP and PERY were recorded in all solvents listed in Table 1, and the spectra in toluene and 2-methyltetrahydrofuran (2-MeTHF) are shown in Figure 4a. Similar to the absorption spectra, the fluorescence spectra of PFP show a small but distinct solvent dependent spectral shift. This behavior is also observed for the fluorescence spectra of PERY (Table 1).

Although the fluorescence spectra of PERY and PFP are similar in energy, the intensity of the PFP emission varies

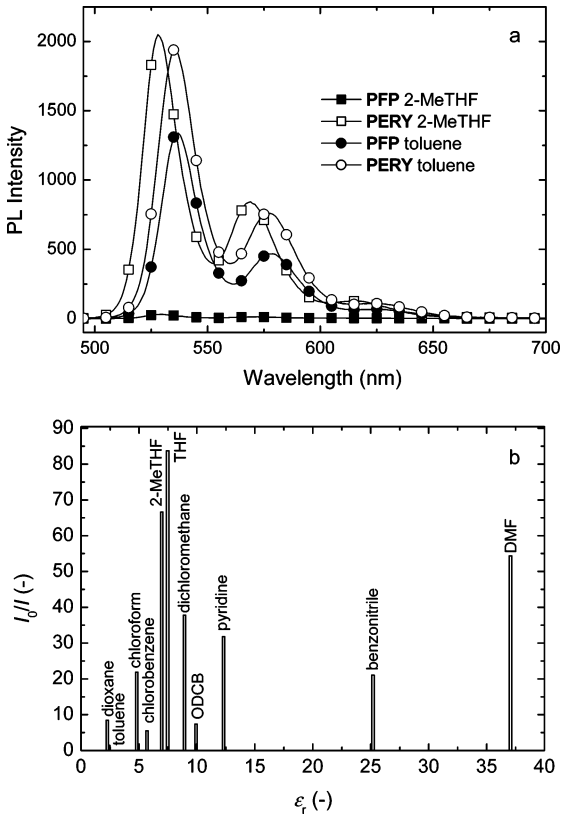

Figure 4. (a) Fluorescence spectra of PFP and PERY in 2-MeTHF and toluene, excited at 490 nm. (b) Fluorescence quenching factor I_0/I versus the relative dielectric constant in different solvents.

strongly with the solvent and is often dramatically reduced compared to that of PERY in the same solvent. The origin of the fluorescence quenching of the perylene bisimide emission in PFP cannot be due to a singlet-energy transfer, because the fluorene S_1 state is much higher in energy. Likewise, quenching via aggregation of the perylene bisimide chromophores is excluded because the UV/vis spectra do not show any sign of aggregation (Figure 2b). Therefore, we can safely attribute the quenching to photoinduced electron transfer in which an electron is transferred from fluorene to perylene bisimide in the S_1 state. Energetically, such electron transfer is not strongly exergonic because the difference between fluorene oxidation and perylene bisimide reduction potentials (1.25 + 1.08 = 2.33 eV in DCM) is very close to the excited state (S_1) energy of perylene bisimide (2.32 eV). Although the redox potentials of perylene bisimide and fluorene in PFP are similar (vide supra), the alternative possibility that an electron transferred from one perylene bisimide unit to another is unlikely as a competing reaction. The electronic coupling between donor and acceptor in the excited state for the latter process will be significantly (orders of magnitude) less because it involves a fluorene bridge rather than directly coupled chromophores. Moreover, charge transfer over larger distances is energetically less favorable because the contribution of the electrostatic potential energy to the charge separated state is higher for larger electron−hole separations. This places the transfer between the perylene bisimides at a higher free energy.

In general, photoinduced electron transfer is more favorable in polar solvents because these stabilize the charge-separated state. Hence, stronger fluorescence quenching was expected for solvents with a higher polar nature. To test this proposition, the extent of fluorescence quenching was measured in the 11 solvents listed in Table 1. For each solvent the fluorescence

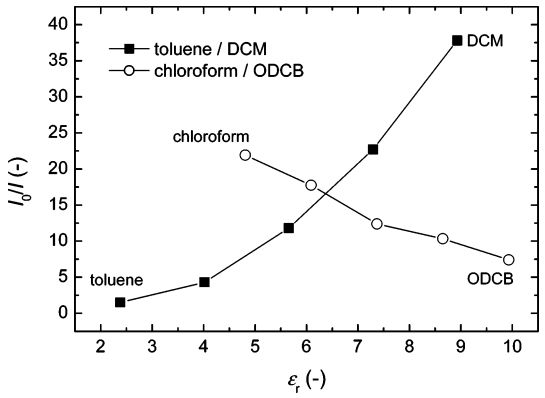

Figure 5. Fluorescence quenching factor I_0/I of PFP in toluene/DCM and chloroform/ODCB solvent mixtures of different composition (0, 25, 50, 75, and 100%) versus the relative dielectric constant of the mixture.

TABLE 2: Rate Constants (k_{CS}, ns^{-1}) for Charge Transfer Obtained from Photoluminescence Quenching (I_0/I) and Photoluminescence Lifetimes (τ_{PFP}, ns) for PFP in Various Solvents

		quenching		lifetime	
	τ_{PERY}	I_0/I	k_{CS}	τ_{PFP}	k_{CS}
dioxane	4.11	8.4	1.8	0.76	1.1
toluene	3.99	1.5	0.13	2.53	0.15
chloroform	3.88	22	5.4	0.12	8.3
chlorobenzene	3.90	5.5	1.2	0.87	0.9
2-MeTHF	3.69	67	17.8	0.04	23.0
THF	4.00	84	20.7	0.05	19.8
DCM	4.39	38	8.4	0.11	8.9
ODCB	3.95	7.4	1.6	0.69	1.2
pyridine	3.91	32	7.9	0.10	10.2
benzonitrile	3.84	21	5.2	0.17	5.6
DMF	4.17	54	12.8	0.07	13.5

quenching factor I_0/I was determined from the fluorescence intensity I of PFP with respect to intensity I_0 of PERY in the same solvent with excitation at the same wavelength. We checked that within the absorption band, the fluorescence quenching was independent of the excitation wavelength, when corrected for differences in absorption. Table 2 clearly shows that the quenching strongly depends on the nature of solvent. For instance, the fluorescence of PFP is quenched by a factor of $I_0/I = 1.5$ in toluene, while in 2-MeTHF the quenching is much stronger with $I_0/I = 67$ (Figure 4a). The extent of quenching observed in dioxane and DMF corresponds well to quenching of a similar compound reported in the literature.[9] Figure 4b shows the fluorescence quenching factor I_0/I of PFP as function of the dielectric constant of the solvent. Figure 4b demonstrates that the extent of quenching is not simply determined by the polarity (represented by the relative dielectric constant) of the solvent.

To investigate the solvent dependence of the fluorescence in more detail, quenching experiments were performed in chloroform/ODCB and toluene/DCM mixtures (Figure 5). The dielectric constants of the solvent mixtures (0, 25, 50, 75, and 100 vol %) were assumed to vary linearly with composition. In both sets of experiments the photoluminescence quenching in the mixtures is between that of the pure solvents, but for toluene/DCM the quenching factor increases with increasing dielectric constant, while it decreases for the chloroform/ODCB mixture. In addition to the opposite trends, we note that the quenching observed for pure solvents with a dielectric constant that is nominally the same as that of the mixtures is also different. This indicates that the extent of quenching of PFP depends on

the solvent but is not (only) determined by the relative dielectric constant. The two sets of experiments clearly show that mixing solvents can lead to ambiguous information with respect to the relation between the dielectric constant and the rate for photoinduced electron transfer.[9,10b]

Fluorescence Lifetime. To study the photoinduced electron transfer in more detail, the fluorescence lifetime of PFP was determined by recording the emission at 534 nm in different solvents with time-correlated single photon counting (TCSPC) after excitation at 400 nm. The fluorescence lifetime of PFP (τ_{PFP}) strongly depends on the solvent, and together with the fluorescence lifetime of PERY (τ_{PERY}) the rate for charge transfer k_{CS} (Table 2) can be estimated via

$$k_{CS} = \frac{1}{\tau_{PFP}} - \frac{1}{\tau_{PERY}} \quad (1)$$

The rate of charge transfer k_{CS} (Table 2) can also be derived from the fluorescence-quenching factor I_0/I

$$k_{CS} = \frac{(I_0/I) - 1}{\tau_{PERY}} \quad (2)$$

For most solvents, the values of k_{CS} obtained from fluorescence lifetime and quenching experiments are similar (Table 2). The rate constant for charge transfer is the largest in THF and the smallest in toluene.

3. Discussion

Energy of the Locally Excited State. The energies of maximum absorption and emission of PFP vary with the nature of the solvent in a similar way as those of the PERY chromophore (Table 1). Since PERY is a symmetrical molecule, it has no net dipole moment in the ground or excited state. The dipole moment of PFP in its ground state is expected to be very small since the molecule does not contain highly polar substituents or groups with a very strongly electron accepting or donating character. Because the solvent shift of the absorption and fluorescence band of PFP is very similar to that of PERY (Figure 6), we conclude that PFP in its perylene bisimide based *local* excited state does not have an appreciable dipole moment. For a molecule without a net dipole moment in the ground and excited state, the solvent dependence of the optical absorption and emission is dominated by dispersion interactions between the dissolved molecule and the surrounding solvent molecules. The solvent-dependence of energy of maximum absorption (or emission) ν is then given by[18]

$$\nu = \nu(0) - \frac{D}{2\pi\epsilon_0 a^3} f' \quad (3)$$

$$f' = \frac{n^2 - 1}{2n^2 + 1} \quad (4)$$

in which $\nu(0)$ is the energy of the absorption (or emission) in the gas phase, a is the radius of the (spherical) solvent cavity needed to store a solute molecule, ϵ_0 is the vacuum permittivity, and n is the refractive index of the solvent. The parameter D describes the difference between the dispersion interactions of the solute molecule in its ground state with the solvent molecules and the interactions of the solute molecule with the solvent in its excited state. A plot of the experimental transition energies ν_{max} for absorption and fluorescence in the different solvents versus f' provides an approximate linear relation (Figure 6), demonstrating that the dispersion interaction is important in the shift of the transition energy.

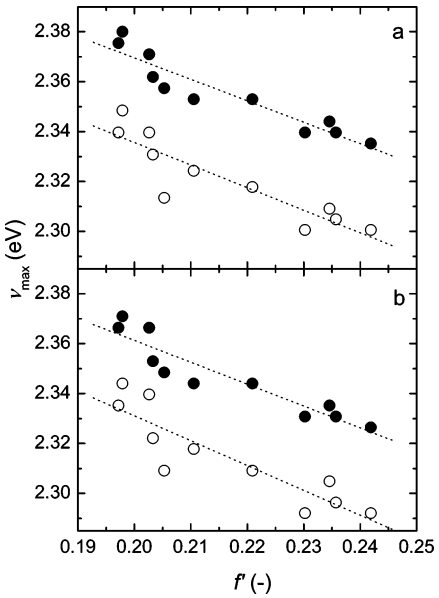

Figure 6. Transition energies ν_{max} of absorption (●) and photoluminescence (○) for PERY (a) and PFP (b) in different solvents vs solvent parameter f'. The slopes of the linear fits are as follows: (a) Abs: −0.86 (± 0.10) eV, PL: −0.90 (± 0.15) eV and (b) Abs: −0.88 (± 0.11) eV, PL: −1.00 (± 0.17) eV.

The average slope of the linear fits are −0.87 eV for absorption and −0.95 eV for emission, and the energy for absorption or emission in a vacuum by extrapolating to $f' = 0$ is $\nu(0) = 2.53$ (±0.05 eV). The radius of the cavity $a = 4.71$ Å of the perylene bisimide was estimated from the density ($\rho = 1.59$ g cm^{-3}) of *N*,*N*′-dimethylperylene-3,4:9,10-tetracarboxylic bisimide as determined from the X-ray crystallographic data via $a = [3M/(4\pi\rho N_A)]^{1/3}$.[19] Using $a = 4.71$ Å, the average slopes give $D = 72$ D^2 for absorption and $D = 79$ D^2 for emission. These values may be compared to those for e.g. naphthalene, where one finds $D = 13$, 41, and 96 D^2 for the ^1L_a, ^1L_b, and ^1B_b states, respectively, and $a = 3.5$ Å.[20]

Charge Transfer. To rationalize the remarkable, and seemingly unpredictable, influence of the solvent polarity on the charge-transfer rate, two related approaches were used: First we use a model that describes the solvent polarization energy contribution to the transition state energy, and in the second approach we use a dielectric continuum model with a spherical cavity to describe the energy of the charge separated state and the Marcus-Jortner model to calculate the rate constant. Both models explain the remarkable dependence of the rate for photoinduced charge separation and the nature of the solvent as shown in Figure 4b.

Polarization Energy in the Transition State. Based on the subnanosecond lifetimes, we consider that the electron transfer reaction proceeds from the relaxed locally excited perylene bisimide state via a transition state to the charge-separated state in a thermally activated reaction. We consider that in the thermal activation step the solvent dipoles need to rearrange to adjust to the dipole moment of the transition state but that the electronic polarization of the solvent molecules can adjust during the Franck−Condon type transition. The contribution of the permanent solvent dipoles to the reaction field F_T associated with a dipole μ_T of the transition state in the center of a spherical

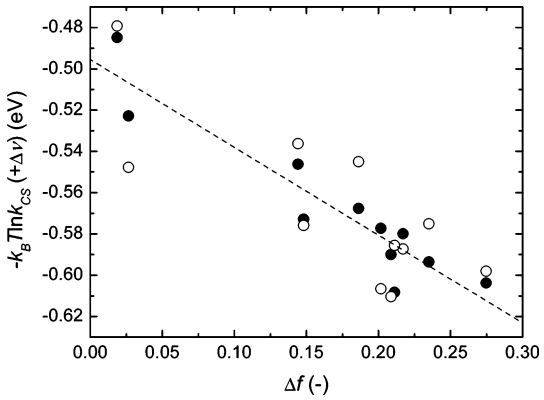

Figure 7. Plots of $-k_BT\ln k_{CS}$ (○) and $-k_BT\ln k_{CS} + \Delta\nu$ (●) versus the solvent parameter Δf. The dashed line is the linear fit to $-k_BT\ln k_{CS} + \Delta\nu$.

cavity with radius a is given by[21,22]

$$\vec{F}_T = \vec{\mu}_T \cdot \frac{1}{2\pi\epsilon_0 a^3}\Delta f \tag{5}$$

$$\Delta f = f - f' = \frac{\epsilon_r - 1}{2\epsilon_r + 1} - \frac{n^2 - 1}{2n^2 + 1} \tag{6}$$

The polarization energy E_{pol} to bring the dielectric into the polarized state associated with the dipole moment of the transition state is[21,22]

$$E_{pol} = \frac{1}{2}\vec{\mu}_T \cdot \vec{F}_T = \frac{{\mu_T}^2 \Delta f}{4\pi\epsilon_0 a^3} \tag{7}$$

The activation energy of the charge transfer $\Delta G_{CS}^{\ddagger}$ can be described by the activation energy in the gas phase $\Delta G_{CS}^{\ddagger}(0)$ minus the polarization energy E_{pol} of the transition state

$$\Delta G_{CS}^{\ddagger} = \Delta G_{CS}^{\ddagger}(0) - \frac{{\mu_T}^2 \Delta f}{4\pi\epsilon_0 a^3} \tag{8}$$

The nonadiabatic charge separation rate constant is a function of the energy barrier $\Delta G_{CS}^{\ddagger}$, the reorganization energy, and the electronic coupling (V) between donor and acceptor in the excited state[23]

$$k_{CS} = \frac{2\pi^{3/2}}{h(\lambda k_B T)^{1/2}} V^2 \exp\left[\frac{-\Delta G_{CS}^{\ddagger}}{k_B T}\right] \tag{9}$$

where λ is total reorganization energy (i.e. the sum of the internal and solvent reorganization energies). Substituting eq 8 into eq 9 shows that rate of charge transfer k_{CS} depends on the solvent parameter Δf via

$$-k_B T\ln k_{CS} = \Delta G_{CS}^{\ddagger}(0) - \frac{{\mu_T}^2 \Delta f}{4\pi\epsilon_0 a^3} - k_B T\ln\left(\frac{V^2}{h}\frac{2\pi^{3/2}}{(\lambda k_B T)^{1/2}}\right) \tag{10}$$

A plot of $-k_BT\ln k_{CS}$ vs Δf (Figure 7, open symbols; k_{CS} taken from the fluorescence quenching) reveals an approximate linear relation with a slope of -0.40 eV ($R = 0.79$). This shows that the last term in eq 10 is not strongly contributing the solvent dependence of k_{CS}.

In eq 10 it assumed that the energy level of the S_1 state is identical in each solvent. The absorption and fluorescence spectra show, however, that the S_1 energy varies significantly with the solvent. When the activation energy is corrected for the changes in S_1 energy ($\Delta\nu = \nu_{max} - \langle\nu\rangle_{av}$, with $\langle\nu\rangle_{av}$ the average of all ν's listed in Table 1), one can write

$$-k_B T\ln k_{CS} + \Delta\nu = \Delta G_{CS}^{\ddagger}(0) - \frac{{\mu_T}^2 \Delta f}{4\pi\epsilon_0 a^3} - k_B T\ln\left(\frac{V^2}{h}\frac{2\pi^{3/2}}{(\lambda k_B T)^{1/2}}\right) \tag{11}$$

As can been seen in Figure 7, a plot of the left-hand term of this expression versus Δf gives a linear relation with a slope of -0.43 eV and an improved correlation coefficient ($R = 0.94$) compared to a fit of $-k_BT\ln k_{CS}$. Considering that electron transfer will occur between the central fluorene and only one of the perylene bisimides, we can estimate the radius of the cavity $a = 5.4$ Å from the molecular volumes calculated from the densities ($V = [M/(\rho N_A)]$) of the perylene bisimide[19] and of fluorene[24] chromophores [$a = (3(V_{pery} + V_{fluorene})/4\pi)^{1/3}$]. This allows for the approximation of the dipole moment in the transition state from the slope of the graphs giving $\mu_T = 10.4$ D and dividing this value by the electron charge, 2.2 Å is obtained as the electron-transfer distance in the transition state.

The important result following from this analysis is that the remarkable solvent dependence of the charge transfer as shown in Figure 3b is dominated by the solvent polarity parameter Δf. Furthermore in the transition state the electron transfer occurs over a small distance only, likely smaller than the radius of the solvent cavity.

Dielectric Continuum Model with a Spherical Cavity. From the above analysis we infer that the center-to-center distance in the electron-transfer reaction in PFP is small and likely less than the sum of the radii of the reactants. When the center-to-center distance between two spherical reactants is less than their radii, the two-sphere model that is often used to describe the energetics and kinetics of charge separation in donor−acceptor systems is not valid,[25,26] and a spherical cavity model is more appropriate. In the one-sphere model, the solvent reorganization energy is described as[27]

$$\lambda_s = \frac{(\Delta\mu)^2}{4\pi\epsilon_0 a^3}\Delta f \tag{12}$$

where $\Delta\mu$ is the magnitude of the difference vector between the dipole moment of the locally excited state μ_{LE} and the dipole moment of the charge-separated state μ_{CS} ($\Delta\mu = |\vec{\mu}_{CS} - \vec{\mu}_{LE}|$). This expression accounts for the nonequilibrium polarization state of the solvent in the charge-separated state. The solvent dependence of the shift in the static energy for the charge separation reaction is[26]

$$\Delta G_{CS} = \Delta G_{CS}(0) - \frac{({\mu_{CS}}^2 - {\mu_{LE}}^2)}{4\pi\epsilon_0 a^3} f \tag{13}$$

where $\Delta G_{CS}(0)$ is the Gibbs free energy in the gas phase. Equations 12 and 13 can be used to calculate the rate of charge transfer k_{CS} by the Marcus−Jortner expression[28]

$$k_{CS} = \left(\frac{\pi}{\hbar^2 \lambda_s k_B T}\right)^{1/2} V^2 \sum_{n=0}^{\infty} e^{-S}\frac{S^n}{n!}\exp\left(-\frac{(\Delta G_{CS} + \lambda_s + n\hbar\omega)^2}{4\lambda_s k_B T}\right) \tag{14}$$

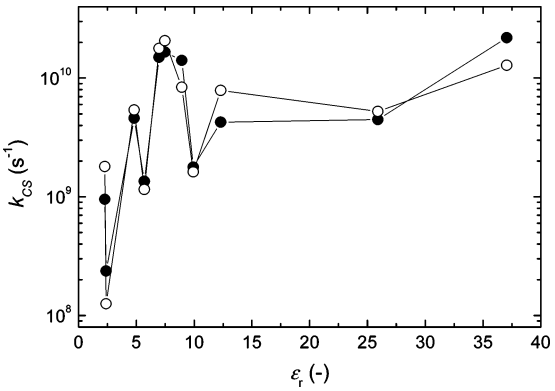

Figure 8. Rate of photoinduced charge transfer k_{CS}, determined from PL quenching experiments (○) and modeled with eqs 12−14 (●) using $\lambda_i = 0.12$ eV, $a = 3.85$ Å, $\Delta G_{CS}(0) = 0$ eV, $(\mu_{CS}^2 - \mu_{LE}^2)^{1/2} = 21.2$ D, $\Delta\mu = 21.8$ D, and $V = 141.1$ cm^{-1}. The values for λ_s are shown in Table 1.[29]

where the Huang−Rhys factor S ($= \lambda_i/h\omega$) relates to the effective mode vibrational energy (taken as $\omega = 1500$ cm^{-1} corresponding to the C=C stretch vibration) and λ_i is the internal reorganization energy. We fitted the experimentally rates of charge separation obtained from the fluorescence quenching in all 11 solvents to the rates given by eqs 12−14, using λ_i, a, $\Delta G_{CS}(0)$, $\Delta\mu$, $(\mu_{CS}^2 - \mu_{LE}^2)$, and V as variables. As a starting point for the optimization we used $\lambda_i = 0.2$ eV, $a = 5.4$ Å, and $\Delta G_{CS}(0) = +0.01$ eV ($= E_{ox} - E_{red} - \nu_{max}$ in DCM) and assumed that $\mu_{LE} = 0$ and $\mu_{CS} = 20$ D (double that of in the transition state μ_T). After optimization the rate constants predicted by the model are in very good agreement with the experimental values within a factor of 2 (Figure 8). The final values of the parameters (see the caption of Figure 8) are close to the starting values.[29] In fact, $(\mu_{CS}^2 - \mu_{LE}^2)^{1/2}$ and $\Delta\mu$ are almost equal confirming that $\mu_{LE} \approx 0$. The result that $\mu_{LE} \approx 0$ is supported by the fact that the solvent dependence of the optical absorption of PFP was found to be dominated by the dispersion interaction (vide supra).

Rationalization of the Continuum Model. The final values of $\Delta G_{CS} + \lambda_s$ (see the Supporting Information) vary from −0.92 eV (for THF and 2-Me-THF) to −1.15 eV for ODCB and reveal that several vibrational quanta ($h\omega$) are required for the reaction to proceed. The remarkable changes in k_{CS} with solvent that have been observed experimentally are the consequence of different effects with a subtle interplay. The shorter distance for charge transfer motivates the use of a spherical model for λ_s (eq 12). Accordingly, the solvent reorganization energy λ_s depends on both ϵ_r and n via the solvent parameter Δf. For aromatic solvents, the generally larger n causes a reduction of λ_s when compared to nonaromatic solvents with similar polarity (compare e.g. DCM and ODCB, Table 1). On the other hand, ΔG_{CS} depends on ϵ_r only and is reduced in more polar solvents. Hence, the free energy and reorganization energies do not scale by similar factors, although both depend on polarity. The importance of the refractive index in determining λ_s becomes clear when considering aromatic vs nonaromatic solvents with similar relative dielectric constant. Looking at three characteristic combinations (viz.: dioxane vs toluene; chloroform vs chlorobenzene; and dichloromethane vs ODCB), the aromatic solvent has a slightly higher ϵ_r, but the higher n and lower λ_s causes a reduction of k_{CS}. Here the model nicely reproduces the observed trends.

As mentioned above, the model does reproduce all rate constants within a factor of 2, while the experimental values differ by more than a factor of 150 for different solvents. On the other hand, some of the differences are not reproduced. As can be seen in Figure 8 (and in Table S1), the model would predict that the charge separation rate constant in DMF (21.9 ns^{-1}) would be larger than in THF (16.6 ns^{-1}), while experimental values are different (12.8 ns^{-1} for DMF versus 20.7 ns^{-1} for THF).

4. Conclusion

Photoinduced charge separation from fluorene to perylene bisimide in PFP occurs with a rate constant k_{CS} varying from $\sim 10^8 - 10^{10}$ s^{-1}, depending on the solvent. The nature of the solvent strongly affects the rate constants, but the rate does not monotonically increase with the relative dielectric constant. In fact we have observed opposite trends with increasing polarity in two different solvent mixtures. The remarkable solvent dependence (Figure 8) can be successfully explained in terms of two related models. In the first model we consider that the polarization energy of the solvent, induced by the dipole moment in the transition energy, affects the activation barrier for charge separation, and we derive that $\ln k_{CS}$ scales linearly with the solvent parameter Δf in accordance with the experiments. In the second model we use the classical Marcus−Jortner equation for charge transfer and employ a spherical cavity model for the reorganization energy which varies linearly with Δf. With this second model we are able to accurately (within a factor 2) describe the widely varying (factor of more than 150) rate of charge separation in PFP for all 11 solvents.

The reason for the exceptional influence of the solvent on the charge separation is the fact that the driving force for the charge separation reaction over long distances is low in each solvent (e.g. in DCM: $E_{ox} - E_{red} - \nu_{max} = +0.01$ eV), causing that the distance over which the electron transfer can take place will be small. At short distances the solvation of the charge separated state is strongly dependent on the solvent, making subtle changes in the medium important. The unique feature of the PFP molecule is that fluorene and perylene bisimide units are directly coupled, allowing for such short distance electrons transfers to occur.

5. Experimental Section

Methods. UV/vis absorption spectra were recorded on a Perkin-Elmer Lambda 900 or a Lambda 40 spectrophotometer. Fluorescence spectra were recorded on an Edinburgh Instruments FS920 double-monochromator spectrometer with a Peltier-cooled red-sensitive photomultiplier. Time-correlated single photon counting fluorescence studies were performed using an Edinburgh Instruments LifeSpec-PS spectrometer, consisting of a 400 nm picosecond laser (PicoQuant PDL 800B) operated at 2.5 MHz and a Peltier-cooled Hamamatsu microchannel plate photomultiplier (R3809U-50). Lifetimes were determined from the data using the Edinburgh Instruments software package.

NMR spectra were recorded at room temperature on a Varian Gemini spectrometer at frequencies of 300 and 75 MHz for ^{1}H and ^{13}C nuclei or a Bruker spectrometer at frequencies of 400 and 100 MHz for ^{1}H and ^{13}C nuclei. Chemical shifts are given in ppm (δ) relative to tetramethylsilane. Matrix assisted laser desorption ionization time-of-flight (MALDI-TOF) mass spectrometry was conducted on a Perseptive Biosystems Voyager DE-Pro MALDI-TOF mass spectrometer. Elemental analysis was carried out on a Perkin-Elmer 2400 series II CHN analyzer.

Preparative HPLC was performed with a Shimadzu system using a LC-8A preparative liquid chromatograph pump (5 mL/min), a SIL-10AD-VP auto injector, a SPD-10AV-VP UV/vis

detector (522 nm), and a SCL-10A-VP system controller, using an eluent gradient of THF/water 8:2 to pure THF. An Alltima C18 5μm column with a length of 150 mm and an internal diameter of 10 mm was used. Cyclic voltammetry was measured in 0.1 M tetrabutylammonium hexafluorophosphate ($TBAPF_6$) as a supporting electrolyte in dichloromethane using an Ecochemie Autolab PGSTAT30 potentiostat. $TBAPF_6$ and DCM were carefully dried prior to the experiments. The working electrode was a Pt disk, the counter electrode was an Ag bar, and an Ag/AgCl electrode was used as reference electrode.

Materials. *N*,*N*′-Bis(1-hexylheptyl)-3,4:9,10-perylenedicarboximide (PERY) and *N*-(1-hexylheptyl)perylene-3,4:9,10-tetracaboxylic-3,4-anhydride-9,10-imide (**4**) were synthesized according to literature procedures.[14,30] All reagents and solvents were commercial products and used as received or purified using standard procedures.

9,9-Didodecylfluorene-2,7-bisphthalimide (2). To dimethylacetamide (dried on molsieves, 50 mL) was added 9,9-didodecyl-2,7-dibromofluorene **1** (2.96 g, 4.48 mmol). After addition of potassium phthalimide (1.66 g, 8.96 mmol) and copper(I) iodide (dried in oven, 1.71 g, 8.96 mmol) the mixture was stirred under argon for five minutes at room temperature and subsequently stirred at 180 °C. After 18 h the reaction mixture was cooled to room temperature and was poured into 4 N HCl (300 mL). To this solution was added CH_2Cl_2, and the organic layer was isolated and subsequently washed with water and brine and dried over Na_2SO_4. After filtration and evaporation of the solvent the product was purified by column chromatography (silica gel, CH_2Cl_2/*n*-hexane 3:1, $R_f = 0.3$). A yellowish/brownish sticky glass was obtained with a yield of 1.00 g (28%). ^{1}H NMR ($CDCl_3$, 300 Hz): 7.98 (dd, $J = 5.5$ Hz, 3.0 Hz, 4H), 7.84 (d, $J = 8.8$ Hz, 2H), 7.81 (dd, $J = 5.5$ Hz, 3.3 Hz, 4H), 7.46 (m, 4H), 2.00−1.95 (m, 4H), 1.30−1.00 (m, 36 H), 0.85−0.70 (m, 10 H). ^{13}C NMR ($CDCl_3$): 167.54, 152.11, 139.97, 134.55, 132.01, 130.89, 125.23, 123.84, 121.46, 120.45, 40.17, 32.05, 30.25, 29.77, 29.72, 29.44, 24.11, 22.82. MALDI-TOF MS (MW = 792.49) $m/z = 793.28$ $[M + H]^+$. Anal. Calcd for $C_{53}H_{62}N_2O_4$: C 80.26, H 8.13, N 3.53. Found: C 79.91, H 7.95, N 3.50.

9,9-Didodecylfluorene-2,7-diamine (3). Compound **2** (0.75 g, 0.95 mmol) and hydrazine monohydrate (0.46 mL, 9.5 mmol) were stirred under argon in refluxing ethanol for 18 h. After this period again hydrazine monohydrate (0.50 mL, 10 mmol) was added, and it was refluxed for another 4 h. After cooling to room temperature, the mixture was filtered, and the solvent was removed in vacuo. The residue was dissolved in diethyl ether and again filtrated. The organic phase was washed with water and brine and dried over Na_2SO_4. After filtration and evaporation of the solvent 0.42 g (83%) of a brown oil was obtained as the product. ^{1}H NMR ($CDCl_3$, 300 MHz) δ 7.33 (dd, $J = 6.3$ Hz, 2.5 Hz, 2H), 6.62 (d, $J = 2.2$ Hz, 2H), 6.61 (d, $J = 6.3$ Hz, 2H), 3.65 (s, 4H), 1.80−1.75 (m, 4H), 1.30−0.95 (m, 36 H), 0.87 (t, $J = 6.9$ Hz, 6H), 0.75−0.60 (br signal, 4H). ^{13}C NMR ($CDCl_3$ 75 MHz): δ 151.63, 144.47, 133.12, 119.01, 113.81, 110.04, 54.59, 40.90, 31.90, 30.23, 29.70, 29.62, 29.38, 29.33, 23.76, 22.68, 14.11. MALDI-TOF MS (MW = 532.48) $m/z = 532.43$ $[M^\bullet]^+$. Anal. Calcd for $C_{37}H_{60}N_2$: C 83.39, H 11.35, N 5.26. Found: C 82.96, H 11.23, N 5.26.

***N*-(1-Hexylheptyl)-*N*′-phenyl-3,4:9,10-perylenedicarboximide (5).**[15] A mixture of *N*-(1-hexylheptyl)perylene-3,4:9,10-tetracaboxylic-3,4-anhydride-9,10-imide **4** (0.2 g, 0.349 mmol), aniline (96 μL, 1.046 mmol), and imidazole (1 g) was stirred for 24 h at 140 °C. The crude product was diluted with CH_2Cl_2 (40 mL) and extracted with water. The organic layer was dried over $MgSO_4$ and evaporated in vacuo. The crude product was purified by silica gel column chromatography (CH_2Cl_2 then CH_2Cl_2/MeOH: 97/3) to give **5** as a reddish solid (167 mg, 74%). ^{1}H NMR ($CDCl_3$) δ 8.72−8.60 (m, 8H), 7.60−7.57 (m, 2H, Ph), 7.53−7.49 (m, 1H, Ph), 7.37 (d, $^3J = 7.2$ Hz, 2H, Ph), 5.18 (hept, $^3J = 6.0$ Hz, 1H, CH), 2.28−2.20 (m, 2H), 1.90−1.85 (m, 2H), 1.32−1.23 (m, 16H, 8 CH_2), 0.83 (t, $^3J = 6.8$ Hz, 6H, CH_3). ^{13}C NMR ($CDCl_3$) δ 163.5, 135.0, 134.2, 131.8, 129.8, 129.6, 129.5, 128.9, 128.58, 126.6, 126.4, 123.3, 123.2, 123.0, 54.8, 32.4, 31.8, 29.2, 26.9, 22.6, 14.0. IR (cm^{-1}): 1697 and 1655 ($\nu_{C=O}$ imide). MALDI-TOF MS (MW = 648.3) $m/z = 648.4$ $[M^\bullet]^-$.

2,7-Bis(*N*-(1-hexylheptyl)-3,4:9,10-perylene-bisimide-*N*′-yl))-9,9-didodecylfluorene (PFP). Diamine **3** (0.34 g, 0.64 mmol), *N*-(1-hexylheptyl)perylene-3,4:9,10-tetracaboxylic-3,4-anhydride-9,10-imide **4** (0.73 g, 1.27 mmol), imidazole (8.85 g), and zinc acetate (0.062 g, 0.34 mmol) were heated to 180 °C and stirred under argon atmosphere. After 16 h no anhydride was present anymore, and the reaction mixture was cooled to room temperature. The reaction mixture was dissolved in CH_2Cl_2 and washed with 2 N HCl and brine. The solution was dried on Na_2SO_4, subsequently filtered, and dried in vacuo. Column chromatography was performed twice (silica gel, (1) CH_2Cl_2 with 0−3% methanol and (2) [a] ethyl acetate, [b] CH_2Cl_2/methanol 95:5, $R_f = 0.95$). The obtained solid was subsequently purified by Soxhlet extraction with ethyl acetate and precipitation from CH_2Cl_2 into ethyl acetate. A red solid (0.25 g, 24%)was obtained, which was around 10% impure according to HPLC characterization. A small amount was purified by preparative HPLC (THF/water) to obtain 12 mg of pure product. ^{1}H NMR ($CDCl_3$, 400 MHz): δ 8.80−8.60 (m, 16H), 7.95 (d, $J = 8.4$ Hz, 2H), 7.40−7.35 (m, 4H), 5.20 (m, 2H), 2.30−2.20 (m, 4H), 2.05−2.00 (m, 4H), 1.95−1.80 (m, 4H), 1.40−1.10 (m, 72H), 1.00−0.95 (m, 4H), 0.84 (m, 18H). ^{13}C NMR ($CDCl_3$, 100 MHz): δ 164.63, 163.59, 152.32, 140.71, 135.03, 134.42, 134.12, 131.80, 131.25, 129.86, 129.58, 127.36, 126.71, 126.47, 124.07, 123.73, 123.54, 123.25, 123.09, 120.70, 55.60, 54.83, 39.98, 32.38, 31.95, 31.76, 30.12, 29.70, 29.67, 29.39, 29.28, 29.21, 26.94, 23.95, 22.69, 22.57, 14.11, 14.03. Mp = 285 °C. MALDI-TOF MS (MW = 1643.96) $m/z = 1644.04$ $[M^\bullet]^-$. Anal. Calcd for $C_{111}H_{126}N_4O_8$: C 81.08, H 7.72, N 3.41. Found: C 80.57, H 7.58, N 3.45.

Acknowledgment. We thank Dr. E. O. Dijk for the optimization routine used. The research was financially supported by The Netherlands Organization for Chemical Research (CW), The Netherlands Organization for Scientific Research (NWO) in the PIONIER program, and the NAIMO EU integrated project (NMP4-CT-2004-500355).

Supporting Information Available: Transient subpicosecond absorption spectroscopy on FPF. This material is available free of charge via the Internet at http://pubs.acs.org.

References and Notes

(1) See, e.g.: (a) Wasielewski, M. R. *Chem. Rev.* **1992**, *92*, 435. (b) Gust, D.; Moore, T. A.; Moore, A. L. *Acc. Chem. Res.* **1993**, *26*, 198. (c) Gray, H. B.; Winkler, J. R. *Annu. Rev. Biochem.* **1996**, *65*, 537. (d) Gust, D.; Moore, T. A.; Moore, A. L. *Acc. Chem. Res.* **2001**, *34*, 40.

(2) See, e.g.: (a) Guldi, D. M. *Chem. Soc. Rev.* **2002**, *31*, 22. (b) Imahori, H.; Mori, Y.; Matano, *J. Photochem. Photobiol. C* **2003**, *4*, 51. (c) Kuciauskas, D.; Liddell, P. A.; Lin, S.; Johnson, T. E.; Weghorn, S. J.; Lindsey, J. S.; Moore, A. L.; Moore, T. A.; Gust, D. *J. Am. Chem. Soc.* **1999,** *121*, 8604. (d) Andersson, M.; Sinks, L. E.; Hayes, R. T.; Zhao, Y.; Wasielewski, M. R. *Angew. Chem., Int. Ed.* **2003**, *42*, 3139

(3) (a) Mihailetchi, V. D.; Blom, P. W. M.; Hummelen, J. C.; Rispens, M. T. J. *Appl. Phys.* **2003**, *94*, 6849. (b) Gadisa, A.; Svensson, M.; Andersson, M. R.; Inganäs, O. *Appl. Phys. Lett.* **2004**, *84*, 1609.

(4) (a) Jäckel, F.; De Feyter, S.; Hofkens, J.; Köhn, F.; De Schryver, F. C.; Ego, C.; Grimsdale, A.; Müllen, K. *Chem. Phys. Lett.* **2002**, *362*, 534. (b) Ego, C.; Marsitzky, D.; Becker, S.; Zhang, J.; Grimsdale, A. C.; Müllen, K.; MacKenzie, J. D.; Silva, C.; Friend, R. H. *J. Am. Chem. Soc.* **2003**, *125*, 437. (c) Ego, C.; Marsitzky, D.; Becker, S.; Zhang, J.; Grimsdale, A. C.; Müllen, K.; MacKenzie, J. D.; Silva, C.; Friend, R. H. *J. Am. Chem. Soc.* **2003**, *125*, 437. (d) Herz, L. M.; Silva, C.; Friend, R. H.; Philips, R. T.; Setayesh, S.; Becker, S.; Marsitsky, D.; Müllen, K. *Phys. Rev. B* **2001**, *64*, 195203. (e) Beljonne, D.; Pourtois, G.; Silva, C.; Hennebicq, E.; Herz, L. M.; Friend, R. H.; Scholes, G. D.; Setayesh, S.; Müllen, K.; Brédas, J. L. *Proc. Natl. Acad. Sci.* **2002**, *99*, 10982. (f) Dudek, S. P.; Pouderoijen, M.; Abbel, R.; Schenning, A. P. H. J.; Meijer, E. W. *J. Am. Chem. Soc.* **2005**, *127*, 11763.

(5) Russell, D. M.; Arias, A. C.; Friend, R. H.; Silva, C.; Ego, C.; Grimsdale, A. C.; Müllen, K. *Appl. Phys. Lett.* **2002**, *80*, 2204.

(6) (a) Belfield, K. D.; Schafer, K. J.; Alexander, M. D. *Chem. Mater.* **2000**, *12*, 1184. (b) Belfield, K. D.; Bondar, M. V.; Przhonska, O. V.; Schafer, K. J. *J. Photochem. Photobiol. A* **2002**, *151*, 7. (c) Ego, C.; Marsitzky, D.; Becker, S.; Zhang, J.; Grimsdale, A. C.; Müllen, K.; MacKenzie, J. D.; Silva, C.; Friend, R. H. *J. Am. Chem. Soc.* **2003**, *125*, 437. (d) Xu, S.; Yang, M.; Bai F. *J. Mater. Sci. Lett.* **2002**, *21*, 1903. (e) Yang, M.-J.; Xu, S.-G. *Synth. Met.* **2003**, *137*, 1099.

(7) Goldsmith, R. H.; Sinks, L. E.; Kelley, R. F.; Betzen, L. J.; Liu, W.; Weiss, E. A.; Ratner, M. A.; Wasielewski, M. R. *Proc. Natl. Acad. Sci.* **2005**, *102*, 3540.

(8) Izquierdo, M. A.; Bell, T. D. M.; Habuchi, S.; Fron, E.; Pilot, R.; Vosch, T.; De Feyter, S.; Verhoeven, J.; Jacob, J.; Müllen, K.; Hofkens, J.; De Schryver, F. C. *Chem. Phys. Lett.* **2005**, *401*, 503.

(9) Holman, M. W.; Yan, P.; Ching, K.-C.; Liu, R.; Ishak, F. I.; Adams, D. M. *Chem. Phys. Lett.* **2005**, *413*, 501.

(10) (a) Liu, R.; Holman, M. W.; Zang, L.; Adams, D. M. *J. Phys. Chem. A* **2003**, *107*, 6522. (b) Holman, M. W.; Liu, R.; Zang, L.; Yan, P.; DiBenedetto, S. A.; Bowers, R. D.; Adams, D. M. *J. Am. Chem. Soc.* **2004**, *126*, 16126.

(11) (a) Ghorai, P. K.; Matyushov, D. V. *J. Phys. Chem. A* **2006**, *110*, 8857. (b) Gupta, S.; Matyushov, D. V. *J. Phys. Chem. A* **2004**, *108*, 2087. (c) Zimmt, M. B.; Waldeck, D. H. *J. Phys. Chem. A* **2003**, *107*, 3580. (d) Small, D. W.; Matyushov, D. V.; Voth, G. A. *J. Am. Chem. Soc.* **2003**, *125*, 7470. (e) Vath, P.; Zimmt, M. B.; Matyushov, D. V.; Voth, G. A. *J. Phys. Chem. B* **1999**, *103*, 9130. (f) Weaver, M. J. *Chem. Rev.* **1992**, *92*, 463.

(12) Bacon, R. G. R.; Karim, A. *J. Chem. Soc., Perkin Trans. 1* **1973**, 272.

(13) Semenov, V. A.; Skorovarov, D. I. *J. Org. Chem. USSR (Eng.)* **1969**, *5*, 39.

(14) Kaiser, H.; Lindner, J.; Langhals, H. *Chem. Ber.* **1991**, *124*, 529.

(15) Langhals, H.; Jona, W. *Chem.—Eur. J.* **1998**, *4*, 2110.

(16) Neuteboom, E. E.; Meskers, S. C. J.; Meijer, E. W.; Janssen, R. A. J. *Macromol. Chem. Phys.* **2004**, *205*, 217.

(17) Hapiot, P.; Lagrost, C.; Le Floch, F.; Raoult, E. Rault-Berthelot, J. *Chem. Mater.* **2005**, *17*, 2003.

(18) (a) Liptay, W. *Z. Naturforsch., A: Phys. Sci.* **1965**, *20a*, 1441. (b) Beens, W.; Knibbe, H. Weller, A. *J. Chem. Phys.* **1967**, *47*, 1183. (c) Liptay, W. *Angew. Chem., Int. Edit.* **1969**, *8*, 177.

(19) Hädicke, E.; Graser, F. *Acta Crystallogr., Sect. C: Cryst. Struct. Commun.* **1986**, *42*, 189.

(20) Weigang, O. E., Jr. *J. Chem. Phys.*. **1960**, *33*, 892.

(21) Böttcher, C. F. J.; Bordewijk, P. *Theory of Electric Polarization*, 2nd ed.; Elsevier: Amsterdam, The Netherlands, 1978.

(22) Beens, H. Ph.D. Thesis, Free University of Amsterdam, Amsterdam, The Netherlands, 1969.

(23) Kroon, J.; Oevering, H.; Verhoeven, J. W.; Warman, J. M.; Oliver, A. M.; Paddon-Row: M. N. *J. Phys. Chem.* **1993**, *97*, 5065.

(24) Bel'skii, V. K.; Zavodnik, V. E.; Vozzhennikov, V. M. *Acta Crystallogr., Sect. C: Cryst. Struct. Commun.* **1984**, *C40*, 1210.

(25) Brunschwig, B. S.; Ehrenson, S.; Sutin, N. *J. Phys. Chem.* **1986**, *90*, 3657.

(26) Liu, M.; Ito, N.; Maroncelli, M.; Waldeck, D. H.; Oliver A. M.; Paddon-Row: M. N. *J. Am. Chem. Soc.* **2005**, *127*, 17867 and references therein.

(27) (a) Lippert, E. *Z. Naturforsch., A: Phys. Sci.* **1955**, *10a*, 541. (b) Mataga, N.; Kaifu, Y.; Koizumi, M. *Bull. Chem. Soc. Jpn.* **1955**, *28*, 69. (c) Mataga, N.; Kubota, T. *Molecular Interactions and Electronic Spectra*; Marcel Dekker: New York, 1970.

(28) (a) Kestner, N. R.; Logan, J.; Jortner, J. *J. Phys. Chem.* **1974**, *78*, 2148. (b) Ulstrup, J.; Jortner, J. *J. Chem. Phys.* **1975**, *63*, 4358.

(29) We note that the fit of the model to the experimental data does not critically depend on the value of $\Delta G_{CS}(0)$. While optimization provides $\Delta G_{CS}(0) = 0$ eV and $V = 141$ cm^{-1}, we found that similarly good fits can be obtained for $\Delta G_{CS}(0)$ in the range -0.20 to $+0.20$ eV and adjusting the electronic coupling V from 375 to 60 cm^{-1}.

(30) Demmig, S.; Langhals, H. *Chem. Ber.* **1988**, *121*, 225.